NASA Technical Memorandum 100074

Hypersonic Blunt Body Computations Including Real Gas Effects

J.-L. Montagné, H. C. Yee, G. H. Klopfer, and M. Vinokur

March 1988

NASA
National Aeronautics and
Space Administration

Hypersonic Blunt Body Computations Including Real Gas Effects

J.-L. Montagné, ONERA, B.P. 72, 92322 Chatillon Cedex, France
H. C. Yee, NASA Ames Research Center, Moffett Field, California
G. H. Klopfer, NEAR Inc., Mountain View, California
M. Vinokur, Sterling Software, Palo Alto, California

NASA

HYPERSONIC BLUNT BODY COMPUTATIONS
INCLUDING REAL GAS EFFECTS

J.-L. Montagné[†]

ONERA, B.P. 72, 92322 Chatillon Cedex, France

H.C. Yee[‡]

NASA Ames Research Center, Moffett Field, CA 94035 USA

G.H. Klopfer[*]

NEAR Inc., Mountain View, CA 94043 USA

and

M. Vinokur[**]

Sterling Software, Palo Alto, CA 94030 USA

I. Motivation and Objective

The recently developed second-order explicit and implicit total variation diminishing (TVD) shock-capturing methods of the Harten and Yee [1,2], Yee [3,4], and van Leer [5,6] types in conjunction with a generalized Roe's approximate Riemann solver of Vinokur [7] and the generalized flux-vector splittings of Vinokur and Montagné [8] for two-dimensional hypersonic real gas flows are studied. A previous study [9] on one-dimensional unsteady problems indicated that these schemes produce good shock-capturing capability and that the state equation does not have a large effect on the general behavior of these methods for a wide range of flow conditions for equilibrium air. The objective of this paper is to investigate the applicability and shock resolution of these schemes for two-dimensional steady-state hypersonic blunt body flows.

The main contribution of this paper is to identify some of the elements and parameters which can affect the convergence rate for high Mach numbers or real gases but have negligible effect for low Mach number cases for steady-state inviscid blunt body flows. In order to investigate these different points, two kinds of flows are considered. The blunt body calculations at Mach numbers higher than 15 allow significant real gas effects to occur, while the case of an impinging shock provides a test on the treatment of slip surfaces and complex shock structures. In separate papers, a temporally second-order, implicit, time-accurate TVD-type algorithm for viscous steady and unsteady flows is studied. Studies show that the behavior of the schemes with various temporal differencing but similar spatial

discretization for inviscid and viscous flows are very different — in terms of stability and convergence rate. This point will be addressed in reference [10]. However, this paper only concerns itself with steady-state inviscid computations.

In the following section, the generalized Roe's approximate Riemann solver and flux-vector splittings for real gases are reviewed. Due to space limitation, only the ADI linearized conservative implicit version of the Harten and Yee schemes [11] and Yee [3] is reviewed here since most of the illustrations are computed with this particular algorithm. The findings concerning the various aspects in improving the convergence rate and numerical examples are discussed in the subsequent sections.

II. Description of the Numerical Algorithm

The conservation laws for the two-dimensional Euler equations can be written in the form

$$\frac{\partial U}{\partial t} + \frac{\partial F(U)}{\partial x} + \frac{\partial G(U)}{\partial y} = 0. \tag{1}$$

where $U = \begin{bmatrix} \rho, & m, & n, & e \end{bmatrix}^T$, $F = \begin{bmatrix} \rho u, & mu+p, & nu, & eu+pu \end{bmatrix}^T$, and $G = \begin{bmatrix} \rho v, & mv, & nv+p, & ev+pv \end{bmatrix}^T$. Here ρ is the density, $m = \rho u$ is the x-component of the momentum per unit volume, $n = \rho v$ is the y-component of the momentum per unit volume, p is the pressure, $e = \rho[\epsilon + \frac{1}{2}(u^2 + v^2)]$ is the total internal energy per unit volume, and ϵ is the specific internal energy.

A generalized coordinate transformation of the form $\xi = \xi(x, y)$ and $\eta = \eta(x, y)$ which maintains the strong conservation-law form of equation (1) is given by

$$\frac{\partial \widehat{U}}{\partial t} + \frac{\partial \widehat{F}(\widehat{U})}{\partial \xi} + \frac{\partial \widehat{G}(\widehat{U})}{\partial \eta} = 0, \tag{2}$$

where $\widehat{U} = U/J$, $\widehat{F} = (\xi_x F + \xi_y G)/J$, $\widehat{G} = (\eta_x F + \eta_y G)/J$, and $J = \xi_x \eta_y - \xi_y \eta_x$, the Jacobian transformation. Let $A = \partial F/\partial U$ and $B = \partial G/\partial U$. Then the Jacobians $\widehat{A} = \partial \widehat{F}/\partial \widehat{U}$ and $\widehat{B} = \partial \widehat{G}/\partial \widehat{U}$ can be written as

$$\widehat{A} = (\xi_x A + \xi_y B) \tag{3a}$$

$$\widehat{B} = (\eta_x A + \eta_y B). \tag{3b}$$

2.1. Riemann Solvers

Here the usual approach of applying the one-dimensional scalar TVD schemes via the so called Riemann solvers for each direction in multidimensional nonlinear systems of hyperbolic conservation laws (see for example reference [2]) is used. The eigenvalues and eigenvectors of the Jacobian matrices $\widehat{A}$ and $\widehat{B}$ are used in approximate Riemann solvers. Given two states whose difference is ΔU, Roe [12] obtained an average $\overline{A}$ in the ξ-direction, for example, satisfying $\Delta \widehat{F} = \overline{A} \Delta U$ for a perfect gas. The generalization by Vinokur [7] for an arbitrary gas involves the pressure derivatives $\chi = (\partial p/\partial \rho)_{\widetilde{\epsilon}}$ and $\kappa = (\partial p/\partial \widetilde{\epsilon})_\rho$, where $\widetilde{\epsilon} = \rho\epsilon$. The relation $c^2 = \chi + \kappa h$ then gives the speed of sound, where $h = \epsilon + p/\rho$. Introducing $H = h + (u^2 + v^2)/2$, Vinokur found the same expressions for $\overline{u}, \overline{v}$ and $\overline{H}$ as for the perfect gas, and that $\overline{\chi}$ and $\overline{\kappa}$ must satisfy

$$\overline{\chi}\Delta\rho + \overline{\kappa}\Delta\widetilde{\epsilon} = \Delta p. \tag{4}$$

Unique values of $\overline{\chi}$ and $\overline{\kappa}$ are obtained by projecting the arithmetic averages of the values for the two states into this relation (see references [7] and [2] for the exact formulas).

Flux-vector splitting methods divide the flux $\widehat{F}$ into several parts, each of which has a Jacobian matrix whose eigenvalues are all of one sign. The approach by Steger and Warming [13] made use of the relation $F = AU$, valid for a perfect gas. Van Leer [6] constructed a different splitting in which the eigenvalues of the split-flux Jacobians are continuous and one of them vanishes leading to sharper capture of transonic shocks. Vinokur and Montagné [8] showed that the expressions for both these splittings can be generalized to an arbitrary gas by using the variable $\gamma = \rho c^2/p$, and adding to the split energy flux a term equal to the product of the split mass flux and the quantity $\epsilon - c^2/\big[\gamma(\gamma - 1)\big]$ (see references [8] and [2] for the exact formulas).

2.2 Description of the Implicit TVD schemes

Let Δt be the time step and let the grid spacing be denoted by $\Delta\xi$ and $\Delta\eta$ such that $\xi = j\Delta\xi$ and $\eta = k\Delta\eta$. An implicit second-order in space, first-order in time TVD algorithm in generalized coordinates of Yee and Harten for two-dimensional systems (1) [2-4] can be written as

$$\widehat{U}_{j,k}^{n+1} + \frac{\Delta t}{\Delta\xi}\big[\widetilde{F}_{j+\frac{1}{2},k}^{n+1} - \widetilde{F}_{j-\frac{1}{2},k}^{n+1}\big] + \frac{\Delta t}{\Delta\eta}\big[\widetilde{G}_{j,k+\frac{1}{2}}^{n+1} - \widetilde{G}_{j,k-\frac{1}{2}}^{n+1}\big] = \widehat{U}_{j,k}^n. \tag{5}$$

The functions $\widetilde{F}_{j+\frac{1}{2},k}$ and $\widetilde{G}_{j,k+\frac{1}{2}}$ are the numerical fluxes in the ξ- and η-directions evaluated at $(j + \frac{1}{2}, k)$ and $(j, k + \frac{1}{2})$, respectively. Typically, $\widetilde{F}_{j+\frac{1}{2},k}$ can be expressed as

$$\widetilde{F}_{j+\frac{1}{2},k} = \frac{1}{2}\big(\widehat{F}_{j,k} + \widehat{F}_{j+1,k} + R_{j+\frac{1}{2}}\Phi_{j+\frac{1}{2}}\big). \tag{6}$$

Here $R_{j+\frac{1}{2}}$ is the eigenvector matrix for $\partial\widehat{F}/\partial U$ evaluated at some symmetric average of $U_{j,k}$ and $U_{j+1,k}$ (for example, Roe average [12] for a perfect gas and generalized Roe average of Vinokur [7] for real gases). Similarly, one can define the numerical flux $\widetilde{G}_{k+\frac{1}{2}}$ in this manner. For viscous steady and unsteady flows, a fully implicit second-order in time and space algorithm (with the same spatial differencing for the convection terms) appears to be more stable and efficient (in terms of convergence rate) than (5). See references [10,14,15] for details.

Second-order Symmetric TVD Scheme: The elements of the $\Phi_{j+\frac{1}{2}}$ in the ξ-direction denoted by $(\phi_{j+\frac{1}{2}}^l)^S$ for a spatially second-order symmetric TVD scheme [3,4] are

$$(\phi_{j+\frac{1}{2}}^l)^S = -\psi(a_{j+\frac{1}{2}}^l)\left[\alpha_{j+\frac{1}{2}}^l - \widehat{Q}_{j+\frac{1}{2}}^l\right]. \tag{7a}$$

The value $a_{j+\frac{1}{2}}^l$ is the characteristic speed a^l for $\partial\widehat{F}/\partial U$ evaluated at some average between $U_{j,k}$ and $U_{j+1,k}$. The function ψ is

$$\psi(z) = \begin{cases} |z| & |z| \geq \delta_1 \\ (z^2 + \delta_1^2)/2\delta_1 & |z| < \delta_1 \end{cases}. \tag{7b}$$

Here $\psi(z)$ in equation (7b) is an entropy correction to $|z|$ where δ_1 is a small positive parameter. For steady-state problems containing strong shock waves, a proper control of the size of δ_1 is very important, especially for hypersonic blunt-body flows. See reference [2] or section III for a discussion. An example of limiter function $\widehat{Q}_{j+\frac{1}{2}}^l$ used in calculations is:

$$\widehat{Q}_{j+\frac{1}{2}}^l = \text{minmod}\left[\alpha_{j-\frac{1}{2}}^l, \alpha_{j+\frac{1}{2}}^l, \alpha_{j+\frac{3}{2}}^l\right]. \tag{7.c}$$

The minmod function of a list of arguments is equal to the smallest number in absolute value if the list of arguments is of the same sign, or is equal to zero if any arguments are of opposite sign. Here $\alpha_{j+\frac{1}{2}}^l$ are elements of

$$\alpha_{j+\frac{1}{2}} = R_{j+\frac{1}{2}}^{-1}(U_{j+1,k} - U_{j,k}). \tag{8}$$

Second-Order Upwind TVD Scheme: The elements of the $\Phi_{j+\frac{1}{2}}$ in the ξ-direction denoted by $\left(\phi_{j+\frac{1}{2}}^l\right)^U$ for a spatially second-order upwind TVD scheme [11,2] are

$$\left(\phi_{j+\frac{1}{2}}^l\right)^U = \frac{1}{2}\psi(a_{j+\frac{1}{2}}^l)(g_{j+1}^l + g_j^l) - \psi(a_{j+\frac{1}{2}}^l + \gamma_{j+\frac{1}{2}}^l)\alpha_{j+\frac{1}{2}}^l. \tag{9a}$$

where

$$\gamma_{j+\frac{1}{2}}^l = \frac{1}{2}\psi(a_{j+\frac{1}{2}}^l)\begin{cases} (g_{j+1}^l - g_j^l)/\alpha_{j+\frac{1}{2}}^l & \alpha_{j+\frac{1}{2}}^l \neq 0 \\ 0 & \alpha_{j+\frac{1}{2}}^l = 0 \end{cases}. \tag{9b}$$

An example of limiter function g_j^l used in calculations is

$$g_j^l = \text{minmod}\left[\alpha_{j-\frac{1}{2}}^l, \alpha_{j+\frac{1}{2}}^l\right]. \tag{9c}$$

A Conservative Linearized ADI Form for Steady-State Applications: A conservative linearized ADI form of equation (5) used mainly for steady-state applications as described in detail in references [3,11], can be written as

$$\left[I + \frac{\Delta t}{\Delta \xi}H_{j+\frac{1}{2},k}^\xi - \frac{\Delta t}{\Delta \xi}H_{j-\frac{1}{2},k}^\xi\right]E^* = -\frac{\Delta t}{\Delta \xi}\left[\widetilde{F}_{j+\frac{1}{2},k}^n - \widetilde{F}_{j-\frac{1}{2},k}^n\right] - \frac{\Delta t}{\Delta \eta}\left[\widetilde{G}_{j,k+\frac{1}{2}}^n - \widetilde{G}_{j,k-\frac{1}{2}}^n\right], \tag{10a}$$

$$\left[I + \frac{\Delta t}{\Delta \eta}H_{j,k+\frac{1}{2}}^\eta - \frac{\Delta t}{\Delta \eta}H_{j,k-\frac{1}{2}}^\eta\right]E = E^*, \tag{10b}$$

$$\widehat{U}^{n+1} = \widehat{U}^n + E, \tag{10c}$$

where

$$H_{j+\frac{1}{2},k}^\xi = \frac{1}{2}\left[\widehat{A}_{j+1,k} - \Omega_{j+\frac{1}{2},k}^\xi\right]^n, \tag{10d}$$

$$H_{j,k+\frac{1}{2}}^\eta = \frac{1}{2}\left[\widehat{B}_{j,k+1} - \Omega_{j,k+\frac{1}{2}}^\eta\right]^n. \tag{10e}$$

The nonstandard notation

$$H_{j+\frac{1}{2},k}^\xi E^* = \frac{1}{2}\left[\widehat{A}_{j+1,k}^n E_{j+1,k}^* - \Omega_{j+\frac{1}{2},k}^\xi E^*\right]^n \tag{10f}$$

is used, and $\Omega_{j+\frac{1}{2},k}^\xi$, $\Omega_{j,k+\frac{1}{2}}^\eta$ can be taken as

$$\Omega_{j+\frac{1}{2},k}^\xi E^* = R_{j+\frac{1}{2},k}\text{diag}\left[\psi(a_{j+\frac{1}{2}}^l)\right]R_{j+\frac{1}{2},k}^{-1}(E_{j+1,k}^* - E_{j,k}^*) \tag{10g}$$

$$\Omega_{j,k+\frac{1}{2}}^\eta E = R_{j,k+\frac{1}{2}}\text{diag}\left[\psi(a_{k+\frac{1}{2}}^l)\right]R_{j,k+\frac{1}{2}}^{-1}(E_{j,k+1} - E_{j,k}). \tag{10h}$$

Here $\widehat{A}_{j+1,k}$ and $\widehat{B}_{j,k+1}$ are (3) evaluated at $(j+1,k)$ and $(j,k+1)$, respectively. The nonconservative linearized implicit form suitable for steady-state calculations [2] is also considered. Numerical

4

study indicated that the latter form appears to be slightly less efficient in terms of convergence rate than the linearized conservative form.

III. Enhancement of Convergence Rate for Hypersonic Flows

The current study indicated that the following three elements can affect the convergence rate at hypersonic speeds: (a) the choice of the entropy correction parameter δ_1, (b) the choice of the dependent variables on which the limiters are applied, and (c) the prevention of unphysical solutions during the initial transient stage.

(a). For blunt-body steady-state flows with $M > 4$, the initial flow conditions at the wall are obtained using the known wall temperature in conjunction with pressures computed from a modified Newtonian expression. Also, for implicit methods a slow startup procedure from freestream boundary conditions is necessary. Most importantly, it is advisable to use δ_1 in equation (7b) as a function of the velocity and sound speed. In particular

$$(\delta_1)_{j+\frac{1}{2}} = \widetilde{\delta}(|u_{j+\frac{1}{2}}| + |v_{j+\frac{1}{2}}| + c_{j+\frac{1}{2}}) \tag{11a}$$

$$(\delta_1)_{k+\frac{1}{2}} = \widetilde{\delta}(|u_{k+\frac{1}{2}}| + |v_{k+\frac{1}{2}}| + c_{k+\frac{1}{2}}) \tag{11b}$$

with $0.05 \leq \widetilde{\delta} \leq 0.25$ appear to be sufficient for the blunt-body flows for $4 \leq M \leq 25$. Equation (11) is written in Cartesian coordinates. In the case of generalized coordinates, the u and v should be replaced by the contravariant velocity components, and one half of the sound speed would be from the ξ-direction and the other half would be from the η-direction. For implicit methods, it is very important to use (11) in $\psi(z)$ on both the implicit and explicit operators. For the implicit operator, numerical experiments showed that the linearized conservative form (10) converges slightly faster than the linearized nonconservative form [11]. It seems also that when the freestream Mach number increases, the convergence rate of the linerarized conservative form (10) is slightly better than a simplified version which replaces $\Omega^\xi_{j+\frac{1}{2},k}$ and $\Omega^\eta_{j,k+\frac{1}{2}}$ of (10g,h) by $\max_l \psi(a^l_{j+\frac{1}{2}})$ and $\max_l \psi(a^l_{k+\frac{1}{2}})$ times the identity matrix.

(b). Higher-order TVD schemes in general involve limiter functions. However, there are options in choosing the types of dependent variables in applying limiters for system cases, in particular for systems in generalized coordinates. The choice of the dependent variables on which limiters are applied can affect the convergence process. In particular, due to the nonuniqueness of the eigenvectors $R_{j+\frac{1}{2}}$, the choice of the characteristic variables on which the limiters are applied play an important role in the convergence rate as the Mach number increases. For moderate Mach numbers, the different choice of the eigenvectors have negligible affect on the convergence rate. However, for large Mach number cases, the magnitudes of all the variables at the jump of the bow shock are not the same. In general, the jumps are much larger for the pressures than for the densities or total energy. Studies indicated that employing the form $R_{j+\frac{1}{2}}$ such that the variation of the α are of the same order of magnitude as for the pressure would be a good choice for hypersonic flows. The form similar to the one used by Gnoffo [16] or Roe and Pike [17] can improve the convergence rate over the ones used in references [4,18].

(c). Due to the large gradients and to the fact that the initial conditions are far from the steady-state physical solution, the path used by the implicit method can go through states with negative pressures if a large time step is employed. A convenient way to overcome the difficulties is to fix a minimum allowed value for the density and the pressure. With this safety check, the scheme allows

5

a much larger time step and converges several times faster. In addition, since the Roe's average state allows the square of the average sound speed $c^2_{j+\frac{1}{2}}$ to lie outside the interval between c^2_j and c^2_{j+1}, $c^2_{j+\frac{1}{2}}$ might be negative even though c^2_j and c^2_{j+1} are positive during the transient stage when the initial conditions are far from the steady-state physical solution. In this case, we replace $c^2_{j+\frac{1}{2}}$ by $\max(c^2_{j+\frac{1}{2}}, \min(c^2_j, c^2_{j+1}))$. This later safety check is in particular helpful for the symmetric TVD algorithm (7).

IV. Numerical Results

The current study on the shock resolution of the various schemes for two-dimensional steady-state blunt-body computations indicates similar trends as the one dimensional study [9]. The main issue appears to be their relative efficiency. Due to extra evaluations per dimension in the curve fitting between the left and right states in a real gas for the van Leer formulation, additional computation is required for the van Leer type schemes than the Harten and Yee [1,2], and Yee [3,4] types of TVD schemes. Here van Leer type schemes refer to the use of the MUSCL approach in conjunction with Roe type approximate Riemann solver [12] or flux-vector splittings [6,13]. Moreover, for steady-state applications, implicit methods are preferred over explicit methods because of the faster convergence rate. In addition, it is easier to obtain a noniterative linearized implicit operator for the Harten and Yee, and Yee type schemes than for the van Leer type schemes. For these reasons, the linearized implicit versions of Harten and Yee [11] and Yee [3] are preferred over the van Leer type schemes.

Resolution of First- and Second-Order schemes: For problems containing complex shock structures, first-order upwind TVD schemes are too diffusive unless extremely fine grids are used. For a blunt-body flow containing a single steady bow shock only, the shock-capturing capability of a first-order upwind TVD scheme seems to be quite adequate if one is interested in the shock resolution only. However, a careful examination of the overall flow field of the density and Mach number contours of the first- and second-order TVD schemes compared with the exact solution (shock-fitting solution) reveals the inaccuracy of the first-order scheme. Figure 1 compares the resolution of the first-order (setting $g^l_j = 0$) and second-order upwind TVD schemes (10) using the Roe approximate Riemann solver [12] with the "exact solution" for a perfect gas ($\gamma = 1.4$) at a freestream Mach number of 10. The computations are performed on a 61×33 adapted grid for the full (half) cylinder, which yields a fairly good bow shock resolution by both schemes. However, the contour levels near the body are significantly shifted with the first-order scheme, while the second-order scheme reproduces almost identical results as the exact solution.

Convergence Rate of Explicit and Implicit TVD Schemes at Hypersonic Speed: The five different second-order TVD methods previously studied [9] in one dimension yield very similar shock-resolution for the blunt-body problem. In particular, for an inviscid blunt-body flow in the hypersonic equilibrium real gas range, the explicit second-order Harten and Yee, and Yee-Roe-Davis type TVD schemes [2-4] using the generalized approximate Riemann solver [7] produce similar shock-resolution but converge slightly faster than an explicit second-order van Leer type scheme using the generalized van Leer flux-vector splitting [8].

The freestream conditions for the current study are $M_\infty = 15$ and 25, $p_\infty = 1.22 \times 10^3\ N/m^2$, $\rho_\infty = 1.88^{-2}\ kg/m^3$, and $T_\infty = 226°K$. The grid size is 61×33 for the full (half) cylinder (figure 2). For the $M_\infty = 25$ case, the shock stand off distance is at approximately fourteen points from the wall on the symmetry axis. The relaxation procedure for the explicit methods employs a second-order Runge-Kutta time-discretization with a CFL of 0.5 (solution not shown). The parameter $\tilde{\delta}$ is set to a constant value of 0.15. Pressure and Mach number contours converge and stabilize after 3000-4000

steps but the convergence rate is much slower for the density (with a 2-3 order of magnitude drop in L_2-norm residual). The bow shock is captured in two to three grid points. The curve fits of Srinivasan et al. [19] are used to generate the thermodynamic properties of the gas.

The same flow condition was tested on the implicit scheme (10). The convergence rate is many times faster. Figures (3) and (4) show the Mach number, density, pressure and κ contours computed by the linearized conservative ADI form of the upwind scheme (10) for Mach numbers 15 and 25. Figure 5 shows the slight advantage of the convergence rate of the linearized conservative implicit TVD scheme (10) over the linearized nonconservative implicit TVD scheme suggested in reference [11]. The convergence rate and shock resolution for the symmetric TVD scheme (10,7) behave similarly. For $M_\infty = 15$ case, the L_2-norm residual stagnated after a drop of four orders of magnitude. In general, for a perfect gas with $10 \leq M_\infty \leq 25$ and a not highly clustered grid, steady-state solutions can be reached in 800 steps with 12 orders of magnitude drop in the L_2-norm residual. However, the convergence rate is at least twice as slow for the real gas counter-part. An important observation for the behavior of the convergence rate for the Mach 15 real gas case is that the discontinuities of the thermodynamic derivatives which exist in the curve fits of Srinivasan et al. [19] might be the major contributing factor. This is evident from figures (3d) and (4d) and from comparing with the convergence rate for the perfect gas result.

Computations of impinging shocks: Figure (6) shows the Mach contours computed by the implicit upwind TVD scheme (10) of an inviscid shock-on-shock interaction on a blunt body in the low hypersonic range. Extensive study on flow fields of this type were reported in references [20-22] for the viscous case. This flow field is typical of what will be experienced by the inlet cowl of the National Aerospace Plane (NASP). The freestream conditions for this flow field are $M_\infty = 4.6$, $p_\infty = 14.93$ N/m^2, $T_\infty = 167°$K, $T_w = 556°$K, and $\gamma = 1.4$ for a perfect gas. An oblique shock with an angle of $20.9°$ relative to the free stream impinges on the bow shock. Various types of interactions occur depending on where the impingement point is located on the bow shock. As shown by the Mach contours, the impinging shock has caused the stagnation point to be moved away from its undisturbed location at the symmetry line. The surface pressures at the new stagnation point can be several times larger than those at the undisturbed location of the stagnation point. In addition, a slip surface emanates from the bow shock and impinging shock intersection point and is intercepted by a shock wave which starts at the upper kink of the bow shock. The interacting shock waves and slip surfaces are confined to a very small region and must be captured accurately by the numerical scheme if the proper surface pressures and heat transfer rates are to be predicted correctly. The 77×77 grid used and the convergence rate computed by the implicit scheme (10) are shown in figure (6). Though the pattern of the flow is significantly more complicated than for the previous cases, the convergence rate remains quite satisfactory. Detailed study of viscous steady and unsteady flow fields of this type using a fully implicit second-order time-accurate scheme [10] of the same numerical flux (6-9) for the convection terms are reported in [10,14,15]. It was found that for viscous computations, the scheme suggested by Yee et al. [10] is more robust than equation (10) which is best suited for steady-state inviscid flows.

IV. Concluding Remarks

Some numerical aspects of the TVD schemes that can affect the convergence rate for hypersonic Mach numbers or real gas flows but have negligible effect on low Mach number or perfect gas flows are identified. Improvements have been made to the various TVD algorithms to speed up the convergence rate in the hypersonic flow regime. Even with the improvement though, the convergence is in general slightly slower for a real gas than for a perfect gas. The nonsmoothness in the curve fits

of Srinivasan et al. may be a major contributing factor in slowing down the convergence rate. Due to extra evaluations per dimension in the curve fitting between the left and right states in a real gas for the van Leer formulation, more computation is required for the van Leer type schemes than for the Harten and Yee, and Yee types of TVD schemes.

Aside from the difference in convergence rate, the numerical results confirm the findings of the one dimensional study. The different methods yield very similar shock-resolution on the blunt body problem with freestream Mach numbers up to 25, and the state equation does not have a large effect on the general behavior of these methods. Further improvements on the ADI relaxation algorithm could speed up the convergence rate even more.

References

[1] A. Harten, On a Class of High Resolution Total-Variation-Stable Finite-Difference Schemes, SIAM J. Num. Anal, **21**, 1-23 (1984).

[2] H.C. Yee, Upwind and Symmetric Shock-Capturing Schemes, NASA TM-89464, May 1987; also to appear, proceedings of the "Seminar on Computational Aerodynamics," Dept. Mech. Engin., University of Calif., Davis, Spring Quarter, 1986.

[3] H.C. Yee, Construction of Explicit and Implicit Symmetric TVD Schemes and Their Applications, J. Comput. Phys., **68**, 151-179 (1987); also NASA TM-86775, July 1985.

[4] H.C. Yee, Numerical Experiments with a Symmetric High-Resolution Shock-Capturing Scheme, Proc. 10th Int. Conf. on Numerical Methods in Fluid Dynamics, June 1986, Beijing, China; also NASA TM-88325, June 1986.

[5] B. van Leer, Towards the Ultimate Conservation Difference Scheme V, A Second-Order Sequel to Godunov's Method, J. Comp. Phys., **32**, 101-136 (1979).

[6] B. van Leer, Flux-Vector Splitting for the Euler Equations, ICASE Report 82-30; Sept., 1982.

[7] M. Vinokur, Generalized Roe Averaging for Real Gas, NASA Contractor Report, in preparation.

[8] M. Vinokur and J.-L. Montagné, Generalized Flux-Vector Splitting for an Equilibrium Gas, NASA contractor report, in preparation.

[9] J.-L. Montagné, H.C. Yee and M. Vinokur, Comparative Study of High-Resolution Shock-Capturing Schemes for Real Gas, NASA TM-86839, July 1987.

[10] H.C. Yee, G.H. Klopfer and J.-L. Montagné, High-Resolution Shock-Capturing Schemes for Inviscid and Viscous Hypersonic Flows, Proceedings of the BAIL V conference, June 20-24, 1988, Shanghai, China, also NASA-TM, April 1988.

[11] H.C. Yee, Linearized Form of Implicit TVD Schemes for Multidimensional Euler and Navier-Stokes Equations, Computers and Mathematics with Applications, **12A**, 413-432 (1986).

[12] P.L. Roe, Approximate Riemann Solvers, Parameter Vectors, and Difference Schemes, J. Comp. Phys., **43**, 357-372 (1981).

[13] J.L. Steger and R.F. Warming, Flux-Vector Splitting of the Inviscid Gasdynamic Equations with Application to Finite Difference Methods, J. Comput. Phys., **40**, 263-293 (1981).

[14] G. Klopfer and Yee, H.C., Viscous Hypersonic Shock on Shock Interaction on Blunt Cowl Lips, AIAA-88-0233, AIAA 26th Aerospace Sciences Meeting, Jan. 11-14, 1988, Reno, Nevada.

[15] G. Klopfer, Yee, H.C. and P. Kutler, Numerical Study of Unsteady Viscous Hypersonic Blunt Body Flows With An Impinging Shock, Proceeding of the 11th International Conference on Numerical Methods in Fluid Dynamics, June 27 - July 1, 1988, Williamsburg, Virginia.

[16] P.A. Gnoffo, R.S. McCandless and H.C. Yee, Enhancements to Program LAURA for Efficient Computation of Three-Dimensional Hypersonic Flow, AIAA Paper 87-0280, Jan. 1987.

[17] P.L. Roe and J. Pike, Efficient Construction and Utilisation of Approximate Riemann Solutions, Computing Methods in Applied Sciences and Engineering, ed. R. Glowinski, North-Holland, Amsterdam, J.-L. Lions, 499-518 (1984).

[18] S. Chakravathy and K.Y. Szema, An Euler Solver for Three-Dimensional Supersonic Flows with Subsonic Pockets, AIAA Paper 85-1703, June 1985.

[19] S. Srinivasan, J.C. Tannehill, K.J. Weilmunster, Simplified Curve Fit for the Thermodynamic Properties of Equilibrium Air, ISU-ERI-Ames 86401; ERI Project 1626; CFD15.

[20] T.L. Holst and J.C. Tannehill, Numerical Computation of Three-Dimensional Viscous Blunt Body Flow Fields with an Impinging Shock, ERI Rept. 75169, 1975, Iowa State University, Ames, Iowa.

[21] J.C. Tannehill, T.L. Holst and J.V. Rakich, Numerical Computation of Two-Dimensional Viscous Blunt Body Flows with an Impinging Shock, AIAA J., **14**(2), 204-211 (1976).

[22] J.C. Tannehill, T.L. Holst and J.V. Rakich, Comparison of a Two-Dimensional Shock Impingement Computation with Experiment, AIAA J., **14**(4), 539-541 (1976).
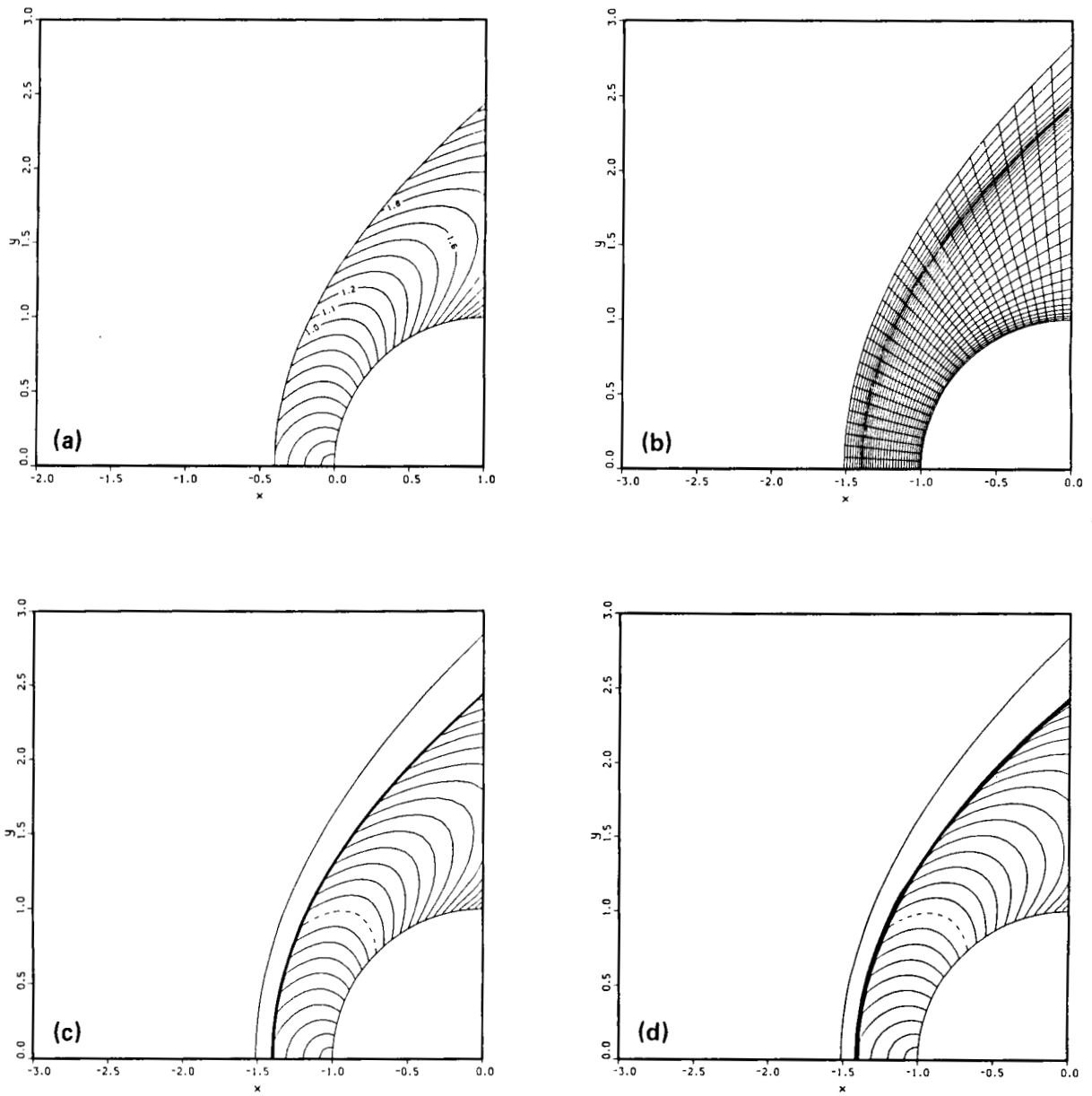
Fig. 1 Comparison among the Mach contours of a second-order implicit upwind TVD scheme (c), a first-order TVD scheme (d) and the shock fitting "exact" solution (a) using the adapted grid (b) for a perfect gas at $M_\infty = 10$.
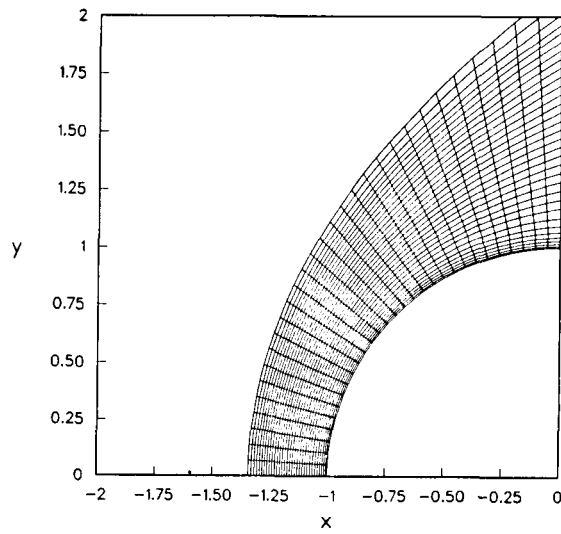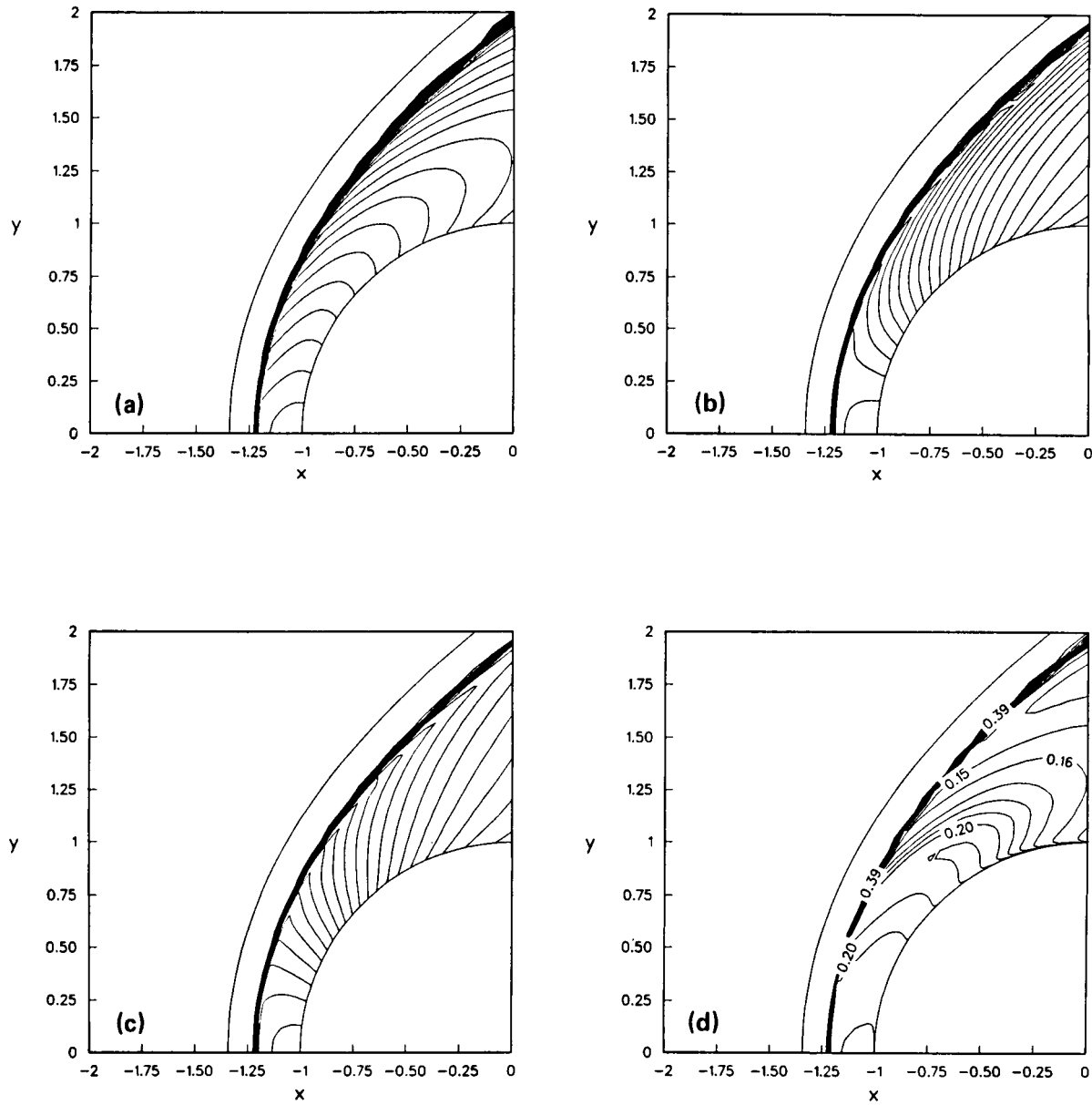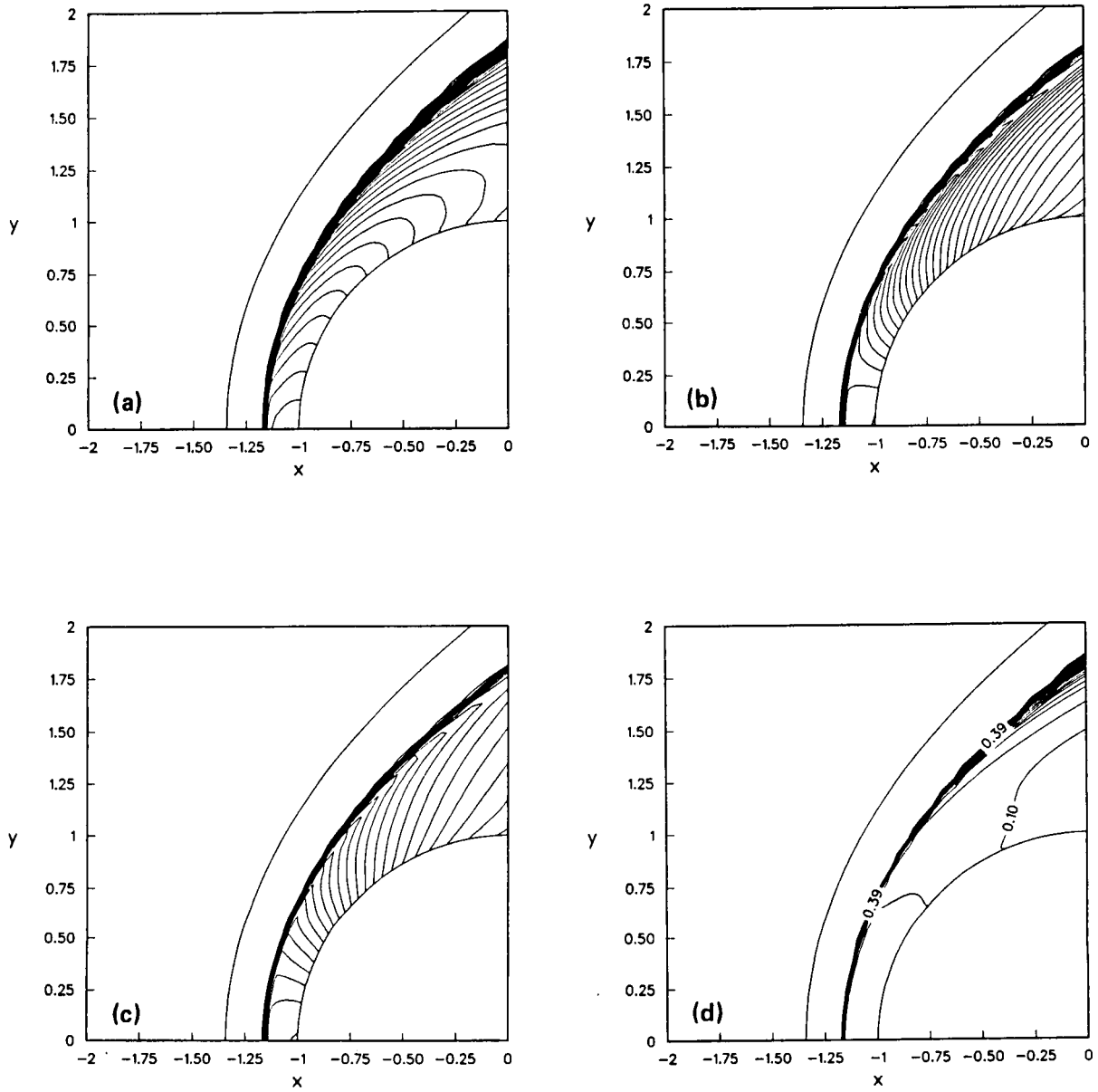
Fig. 2 The 31 × 33 grid.

Fig. 3 The Mach contours (a), density contours (b), pressure contours (c) and κ (d) computed by a second-order implicit TVD scheme for an equilibrium real gas at $M_\infty = 15$.
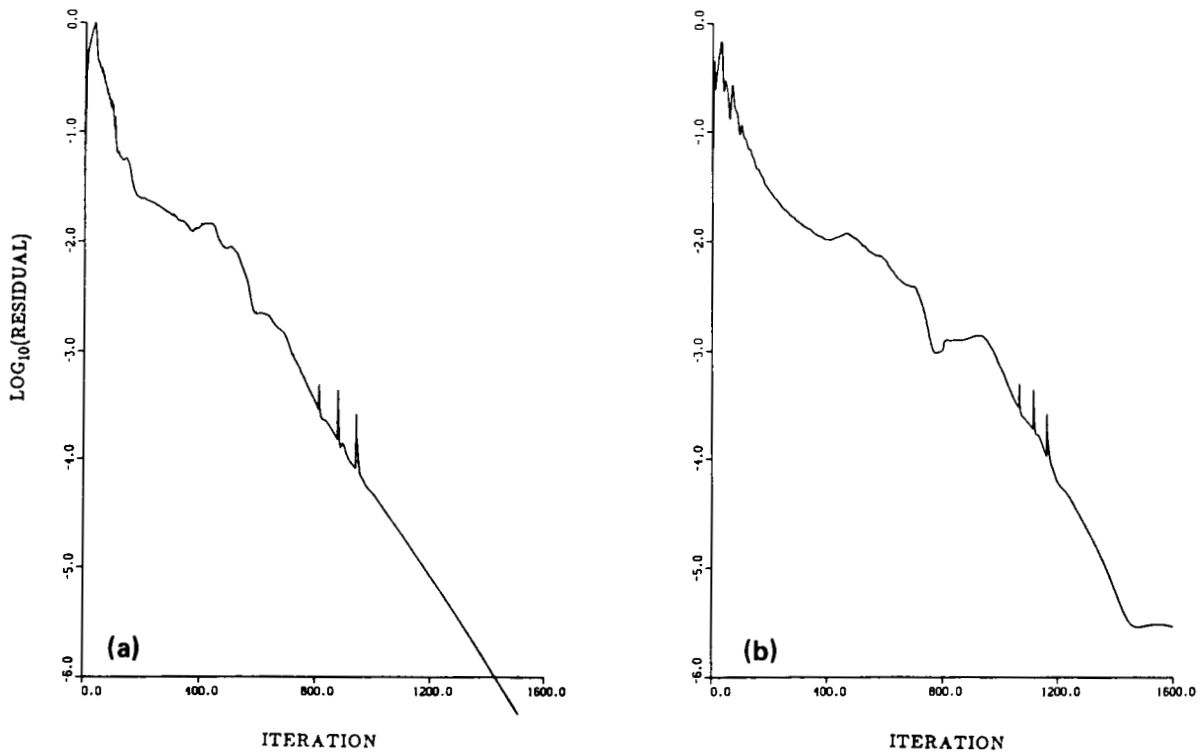
12

Fig. 4 The Mach contours (a), density contours (b), pressure contours (c) and κ (d) computed by a second-order implicit TVD scheme for an equilibrium real gas at $M_\infty = 25$.
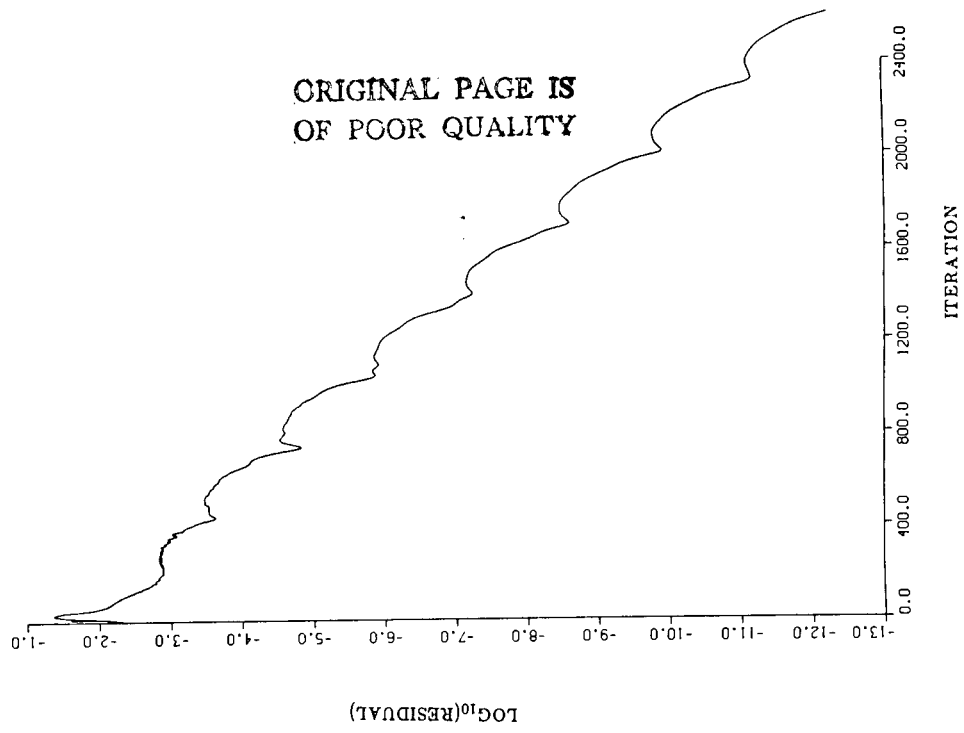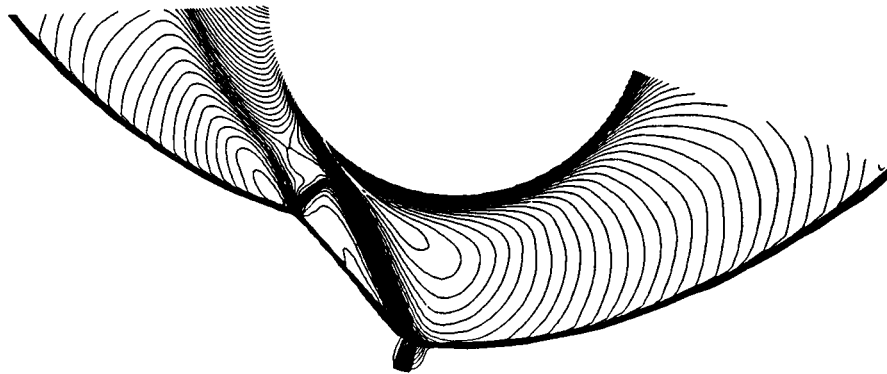
Fig. 5 Comparison of the L_2-norm residual of a linearized conservative implicit operator (a) and a linearized nonconservative implicit operator (b) for an equilibrium real gas at $M_\infty = 25$.
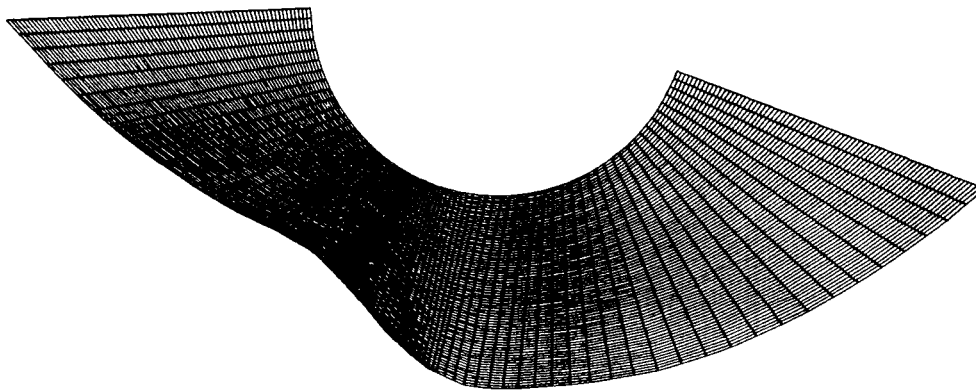
14

CONVERGENCE RATE

MACH CONTOURS

GRID

Fig. 6 Two-dimensional inviscid blunt-body flow computed by a second-order implicit scheme for a perfect gas at $M_\infty = 4.6$.

15

NASA
National Aeronautics and
Space Administration

Report Documentation Page

1. Report No. NASA TM-100074	2. Government Accession No.	3. Recipient's Catalog No.
4. Title and Subtitle Hypersonic Blunt Body Computations Including Real Gas Effects		5. Report Date March 1988
		6. Performing Organization Code
7. Author(s) J.-L. Montagné, H. C. Yee, G. H. Klopfer, and M. Vinokur		8. Performing Organization Report No. A-88109
		10. Work Unit No. 505-60
9. Performing Organization Name and Address Ames Research Center Moffett Field, CA 94035		11. Contract or Grant No.
		13. Type of Report and Period Covered Technical Memorandum
12. Sponsoring Agency Name and Address National Aeronautics and Space Administration Washington, DC 20546-0001		14. Sponsoring Agency Code

15. Supplementary Notes

16. Abstract

The recently developed second-order explicit and implicit total variation diminishing (TVD) shock-capturing methods of the Harten and Yee, Yee, and van Leer types in conjunction with a generalized Roe's approximate Riemann solver of Vinokur and the generalized flux-vector splittings of Vinokur and Montagné for two-dimensional hypersonic real gas flows are studied. A previous study on one-dimensional unsteady problems indicated that these schemes produce good shock-capturing capability and that the state equation does not have a large effect on the general behavior of these methods for a wide range of flow conditions for equilibrium air. The objective of this paper is to investigate the applicability and shock resolution of these schemes for two-dimensional steady-state hypersonic blunt body flows. The main contribution of this paper is to identify some of the elements and parameters which can affect the convergence rate for high Mach numbers or real gases but have negligible effect for low Mach number cases for steady-state inviscid blunt body flows.

17. Key Words (Suggested by Author(s)) Finite difference methods Total variation diminishing schemes (TVD) Real gas flows Blunt body flows	18. Distribution Statement Unclassified — Unlimited Subject Category — 64

19. Security Classif. (of this report) Unclassified	20. Security Classif. (of this page) Unclassified	21. No. of pages 16	22. Price A02

NASA FORM 1626 OCT 86